Integration of Energy Storage Systems based on transcritical CO_2: Concept of CO_2 based Electrothermal Energy and Geological Storage

A. Carro[a], R. Chacartegui[a], C. Ortiz[b], J. Carneiro[c], J.A. Becerra[a]

[a] Dpto. Ingeniería Energética, Escuela Técnica Superior de Ingeniería. Universidad de Sevilla, Camino de los Descubrimientos s/n, 41092 Sevilla, Spain

[b] Universidad Loyola Andalucía, Av. de las Universidades s/n, Dos Hermanas, 41704 Sevilla, Spain

[c] ICT – Departamento de Geociências, Escola de Ciências e Tecnologia, Universidade de Évora, Rua Romão Ramalho, 59, 7000-671 Évora, Portugal

ABSTRACT

Energy storage systems are crucial for the massive deployment of renewable energy at large scale. This paper presents a conceptual large-scale thermoelectrical energy storage system based on a transcritical CO_2 cycle. The concept is developed through the analysis of three high-performance systems: renewable energy storage using a thermoelectric energy storage system, based on a reversible heat pump; a CO_2 storage system; and a novel integration of energy storage using a reversible heat pump and geological injection of CO_2. The latter system efficiently integrates energy and CO_2 storage, taking advantage of the synergies between the operational requirements of both systems. The system uses CO_2 captured in stationary sources as a working fluid for the storage of energy from renewables. The energy is stored and recovered in geological formation and heat/cold tanks, with energy storage based on water and ice sensible heat. A fraction of the CO_2 is expected to be permanently sequestered in the geological formation, adding value to the system. The analysis of the time evolution of the system, under different operation profiles, shows the interest of the concept as a feasible integration for energy storage and CO_2 capture based on renewable energy, with an electric-to-electric efficiency around 50%.

KEYWORDS

Thermoelectric Energy Storage, Transcritical CO_2, Geological Storage, TES, Renewable Energy

NOMENCLATURE

AACAES	Advanced Adiabatic CAES
AL-TES	Aquifer Low-Temperature Storage
ARRD	Availability Renewable Resource and variable Demand
CAES	Compressed Air Energy Storage
CCU	Carbon Capture and Utilisation
CEEGSS	CO_2 based Electrothermal Energy and Geological Storage System
CES	Cryogenic Energy Storage
CO_2	Carbon Dioxide
COP	Coefficient of performance
EESS	Electrothermal Energy Storage System
EOR	Enhanced Oil Recovery
ESS	Energy Storage System
GSS	Geological Storage System
HE	Heat Engine
HP	Heat Pump
HPE	Hourly Price of Electricity
HT	High Temperature
HXI	Heat Exchange – Ice tank

HXW	Heat Exchange – Water tank
LT	Low Temperature
PCM	Phase Change Material
PHS	Pumped Hydroelectric Storage
RTIL	Room Temperature Ionic Liquids
TCES	Thermochemical Energy Storage
TEES	Thermoelectric Energy Storage
TES	Thermal Energy Storage

1. INTRODUCTION

Power generation from renewable resources has increased considerably in recent years [1]. Due to the stochastic and non-continuous nature of renewable resource availability (wind, solar, others), electrical energy storage is one of the main challenges for large-scale renewable power plants integration into the electric grid [2]. Such variability can adversely affect the power quality and electrical grid stability [3]. The development of energy storage systems at different scales, with a satisfactory operation and answering to their specific demand characteristics is needed for advancing towards an electrified system with a high share of renewables [4].

Depending on the amount of energy stored and the speed at which the energy can be stored and/or released, there are different types of energy storage systems. On the small energy scale, there are supercapacitors [5] and flywheels [6], with a very high charge/discharge speed, of the order of seconds, and electrochemical batteries [7], with a wider operating range, from minutes to several days. Electrochemical batteries are currently the most developed technology at kW-scale [4]. Despite the significant cost reduction of batteries in the last years, the price is still an order of magnitude higher than for thermal storage [8]. Thus, batteries are not yet competitive for several hours of storage at a large scale [9]. Medium-size electrical energy storage, like flow batteries [10] and hydrogen fuel cells [11] are being intensively investigated.

On large-scale energy storage, there are few available technologies [9]. Among them stand out pumping hydroelectric energy (PHS) [12], Compressed Air Energy Storage [13] (CAES) systems, and thermal storage systems [14]. PHS is a mature technology with large volume, long storage period, high efficiency and relatively low capital cost per unit of energy. It is the most widely implemented system. However, its application is limited to the availability of water reservoirs with enough altitude difference. CAES is also a commercially available technology capable of providing large energy storage. Characterised by a long storage period, low capital costs and high efficiency, they can respond to load variations because they are designed to sustain frequent on/off cycles. The main obstacle for CAES systems, as in PHS, is the dependence on favourable geological conditions, namely the existence of salt layers and salt domes. Besides, it includes the integration with fossil fuel combustion technologies, with associated emissions [15]. Some improved CAES systems have been proposed [16], including small-scale CAES with small vessels or Advanced Adiabatic CAES with Energy Storage [17]. Both types of Energy Storage Systems (ESS) are based on the transformation of electrical energy into mechanical energy, storing potential energy. Together with these systems, in the context of large-scale energy storage is also thermal energy storage, with a broad spectrum of applications. It is characterised by relatively low efficiency and reduced environmental impact [18]. Depending on whether the operating temperature of the energy storage material is higher than the ambient temperature, they can be classified into low-temperature storage - Aquifer Low-Temperature Storage [19], and Cryogenic Energy Storage [20] (CES) - and high-temperature storage - Room Temperature Ionic Liquids [21], sensible heat systems [22], concrete storage [23] and Phase Change Materials [24].

In all these large-scale storage technologies, their integration with renewables has been investigated, as in the study by Javed et al. [25], where they propose the integration of solar and wind and PHS. In CAES, Rahmanifard and Plaksina [26] simulated a hybrid CAES for wind and solar systems in Alberta, and Ramadan et al. [13] studied the integration of CAES in wind farms in Egypt. TES integrations have been studied by Cetin et al. [20], that studied the use of geothermal energy to be stored with CES; Ochs et al. [14] planned the construction of a hot water

TES for district heating systems; while Prieto and Cabeza [24] analysed the use of PCM in solar plants.

Several options are gaining attention in the last years for storing electricity in thermal systems based on a combination of heat pump and heat engine. Some authors are using the terminology Carnot Batteries for these combinations [27]. Marguerre [28], already presented the idea of the reversible heat pump and the operation of thermal engines for energy storage in 1924, when a system that stored energy both in the form of heat and in the form of compression work was proposed. The idea, which forms the basis of what Merchangoz later defined as thermoelectric energy storage, reappears in a 1978 patent application by Cahn [29,30]. Merchangoz et al. [31] presented a new concept of large scale electricity storage based on the combination of heat pump and heat engine technologies using transcritical CO_2 cycles, and sensible/latent heat storage in hot water, and ice generation and melting. This proposal has been supported by numerous subsequent publications, such as the work by Fernandez et al. [32], the studies by Hao et al. [33,34], or the integration of a solar plant by Tesio et al. [35]. As an alternative, ESS thought Thermochemical Energy Storage (TCES) systems was proposed by Fernandez et al. [36]. The use of CO_2 in storage systems has been proposed in systems with a similar concept that CAES systems [37], and with CO_2 Earth storage [38], or CO_2 storage in aquifers [39].

In this paper, an energy storage system based on transcritical CO_2 cycles is presented. This system is based on the concept of electrothermal energy storage [31] and its integration with geological CO_2 storage [40]. New feasible energy storage technologies are needed in the future electricity systems [40], where electricity storage will allow massive integration of renewables in the grid meanwhile providing greater efficiency of the whole system and increasing the security of the whole electrical system. Currently, renewable energy storage and carbon capture and storage are two critical factors in the fight against climate change. The promotion of CO_2-based systems can support the possible transition to a 100% renewable energy, which is already being investigated in Europe [41].

2. TRANSCRITICAL CO_2 SYSTEM FOR ENERGY STORAGE

2.1 Electrothermal ESS Concept

The thermoelectric energy storage system [32] based on transcritical CO_2 cycles is composed of two closed cycles of CO_2, indirectly connected by a hot and cold thermal storage tanks. This concept of thermoelectric energy storage [31] has already been used in applications as a heat pump to reheat gas in an underground storage system [33].

Figure 1 shows the conceptual system operation: in periods of excess energy, it is stored by a heat pump that compresses CO_2 [32], in figure 1, sequence 1-2-3-4. It transforms electrical energy into thermal energy and stores it. In periods with net electrical demand, the cycle follows in figure 1 the sequence 5-6-7-8, in which thermal energy is transformed into electrical energy by the operation of a CO_2 heat engine.

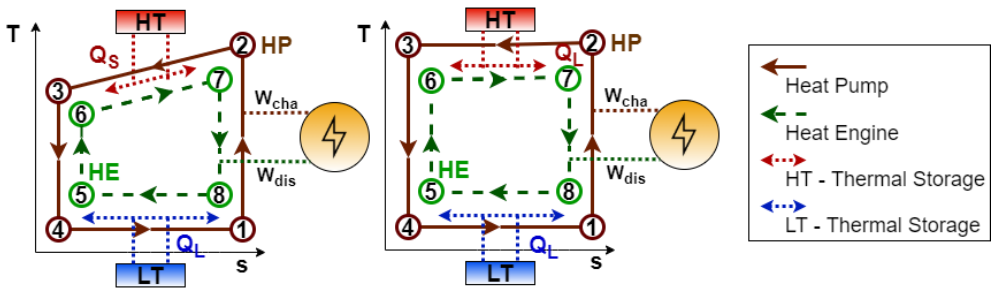

Figure 1. TEES with transcritical cycles concept with well-integrated temperature profiles. HT: High-Temperature; LT: Low-Temperature; QS: Sensible Heat; QL: Latent Heat; W: Work; cha: Charge; dis: Discharge.

Merchangoz et al. [31] proposed CO_2 as a working fluid, characterised by a very low critical temperature, which allows the application of the transcritical cycle in the temperature range of operation and also mentioned that CO_2 as a working fluid has excellent thermal and environmental properties, and is not flammable or toxic.

A functional heat transfer integration with heat storage tanks is required to obtain high efficiency in the operation of the system. During charging, the temperature of the working fluid has to be above the storage temperature during the whole heat transfer process. Figure 1 illustrates two examples of good thermal integration with the parallel evolution of charge-discharge temperature profiles in the heat exchange with thermal storage.

Water is proposed for thermal storage due to its high calorific capacity, its thermal properties, its excellent cost and availability, as well as its safety properties [31]. In the case of low-temperature storage, ice is chosen due to its low price and the attractive potential to take advantage of its sensible and latent heat for thermal energy storage. Cold storage based on ice accounts for 2% of all thermal storage systems [42], and it has been already developed at large scale (up to 50MWh) [43]. An ice slurry technology could be considered as a possible option to improve the cold system performance [44,45]. In this work is considered the use of sensible heat for ice storage. Transcritical CO_2 as working fluid fits hot and cold-water storage temperatures, with favourable heat exchange profiles in both charge/discharge processes.

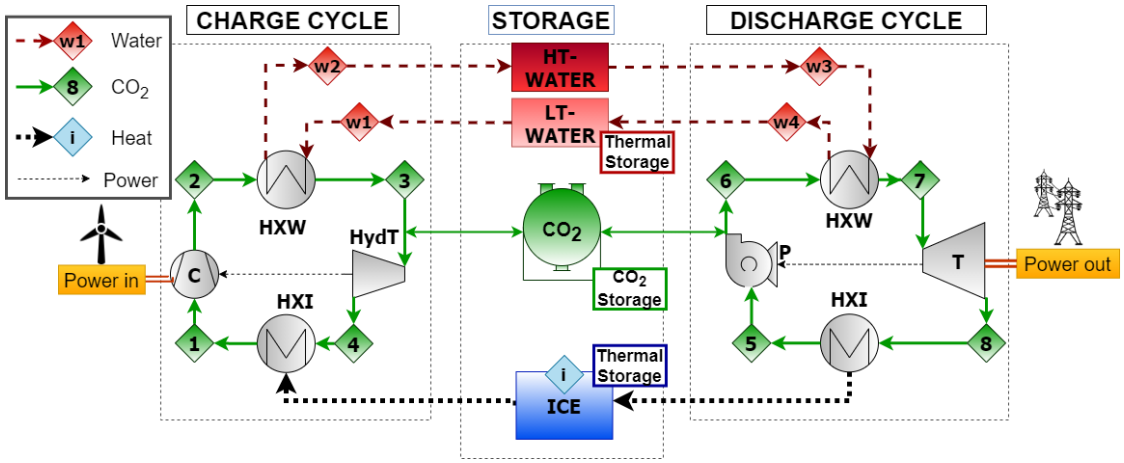

Figure 2. Conceptual layout of the Electrothermal Energy Storage System (EESS). C: Compressor; HydT: Hydraulic turbine; P: Pump; T: Turbine; HXW: Heat exchange – Water; HXI: Heat exchange – Ice; HT: High Temperature; LT: Low temperature.

A conceptual layout of the complete Electrothermal Energy Storage System hereinafter referred to as EESS, is represented in Figure 2. The thermodynamic charging cycle starts at the compressor inlet, where the fluid is compressed, reaching the highest temperature of the whole process. After giving heat to the hot water tank, the fluid expands in a hydraulic turbine, in whose output the lowest temperature of the process is reached. Similarly, the discharge cycle begins at the pump inlet, where the working fluid is compressed. After the evaporator, it expands in a gas turbine. Evolution of CO_2 along the process is shown on the T-s diagram in Figure 8.

2.2 Electrothermal ESS Model

A thermodynamic model has been developed using the commercial software Engineering Equation Solver [46]. Table 1 shows the main assumptions taken. Pressurised water at 100 bar and 15ºC is assumed at point 1 (low-temperature tank) to keep the water in a liquid state when heated above 100ºC (at a pressure of 100 bars the fluid enters the saturation hood at about 300ºC). The initial temperature of the ice is set at -5ºC, a temperature close to that of the saturated liquid. Ice energy storage is based on sensible heat within the temperature range (-15ºC, -5ºC). In this

range the pressure of the ice is not relevant, as it has almost no effect on the melting temperature until very high pressures are reached.

Table 1. Main assumptions and inputs on the EESS modelling (see Figure 2). HP: High-Pressure; LP: Low-Pressure

Parameter	Equipment	Unit	Value
Turbomachinery isentropic efficiency	Compressor		0.86
	Hydraulic turbine		0.85
	Pump		0.85
	Turbine		0.88
Initial conditions in tanks	Water-Pressure	[bar]	100
	Water-Temperature	[ºC]	15
	Ice-Pressure	[bar]	100
	Ice-Temperature	[ºC]	-5
Modelling input parameters	CO_2 quality - compressor		1
	CO_2 quality - pump		0
Heat exchangers	design pinch point	[ºC]	4
Pressure in cycles	HP of CO_2 in charge	[bar]	200
	LP of CO_2 in charge	[bar]	35
	HP of CO_2 in discharge	[bar]	190
	LP of CO_2 in discharge	[bar]	20

The most influential parameters on the cycle performance are the high and low pressure of each cycle. Each cycle consists of two isobaric processes, one for heating and the other for cooling CO_2, and therefore the whole cycle is defined by four pressures. From some initial pressure values [31], the first optimisation of an electrothermal energy storage system with two transcritical CO_2 cycles is made, with which a maximum efficiency of 60% is obtained [47]. These pressure values are used as a starting point in a parametric analysis, in which the evolution of different parameters such as efficiency, heat and work, temperature differences, incompatibilities in the heat exchanges are studied.

The cycles and the overall system performances are evaluated in terms of the indicators defined in equations 1 to 3 corresponding to the charge cycle (COP_{HP}), discharge (η_{HE}) cycle and global (η).

$$COP_{HP} = \frac{\dot{Q}_{HXW} + \dot{Q}_{HXI}}{\dot{W}_C - \dot{W}_{HydT}} \quad (1)$$

$$\eta_{HE} = \frac{\dot{W}_T + \dot{W}_P}{\dot{Q}_{HXW} - \dot{Q}_{HXI}} \quad (2)$$

$$\eta = \frac{\dot{W}_T + \dot{W}_P}{\dot{W}_C - \dot{W}_{HydT}} \quad (3)$$

Where $\dot{Q}_{HXW}, \dot{Q}_{HXI}$ are the heat power in water and ice heat exchangers, respectively, $\dot{W}_C, \dot{W}_{HydT}, \dot{W}_T, \dot{W}_P$ are the power in the compressor, hydraulic turbine, thermal turbine and pump.

3. GEOLOGICAL CO_2 STORAGE SYSTEM USING TRANSCRITICAL CO_2 CYCLES

3.1 Inclusion of geological storage in the concept of Electrothermal ESS

Different integration of CO_2 cycles in energy storage systems have been previously proposed, such as novel fossil-fuel-free trans-critical energy storage system, that uses CO_2 as the working fluid between two saline aquifers or caverns at different depths [34]. In compressed gas-based energy storage, the use of CO_2 as a working medium successfully offers a green solution to carbon capture and storage [38], typically as an alternative to the injection of CO_2 into underground formations such as aquifers [34,39], and other cavities [33]. After capture, the CO_2 must be stored for an extended period. Among the different CO_2 storage options, geological formations are the

cheapest and most environmentally acceptable option [48]. Transport to the storage site can be by pipeline, and its costs depend on the distance and the amount of CO_2 transported. Having CO_2 in a supercritical state is considered the most viable option for this transport, as deduced from the EOR projects [48], because of a reduced specific volume and compression work.

In the present work, we propose the integration of an ESS and geological storage of CO_2 based on renewable energy, within a CCU application, as shown in Figure 3. CO_2 captured in a power plant, or industrial facility is used as a working fluid in the proposed thermodynamic cycle for the storage of renewable electrical energy previously to be stored underground.

The technique is similar to compressed air energy storage (CAES). However, when using CO_2 instead of air, there are some added advantages: improved working fluid properties (low supercritical temperature and moderate pressure), lateral migration (definitive CO_2 sequestration is a benefit resulting from the technique), less geological constraints (migration or residual CO_2 capture functions as a strength for the technique), CO_2 thermosiphon effects (the fluid heats up, expands and decreases in density), which reduces the cost of injecting and producing CO_2 in the wells, as natural circulation and extraction of geothermal heat occur, adding some (minor) geothermal heat to mechanical energy storage, and higher storage density.

The storage of energy occurs in mechanical (work) and thermal (heat) form. Since the geological reservoir needs to be at considerable depth and given the properties of CO_2, a small geothermal heat gain will occur during the charge-discharge phase, which will add to the energy that can be recovered through the expansion of CO_2 in a turbine. Some of the injected CO_2 will migrate laterally from the production wells or will be immobilised by residual trapping, allowing for a continuous supply of CO_2 from a stationary source (CO_2 capture) and fixing part of the involved CO_2. Simulations show that during the operation stage, the CO_2 fluctuates by buoyancy in the geological reservoir, where the CO_2 saturation decreases and CO_2 bubble generally moves to the central and lower parts of the reservoir rather than the outside direction. The system itself effectively alleviates the loss of CO_2 mass from the sidewalls of the reservoir [39].

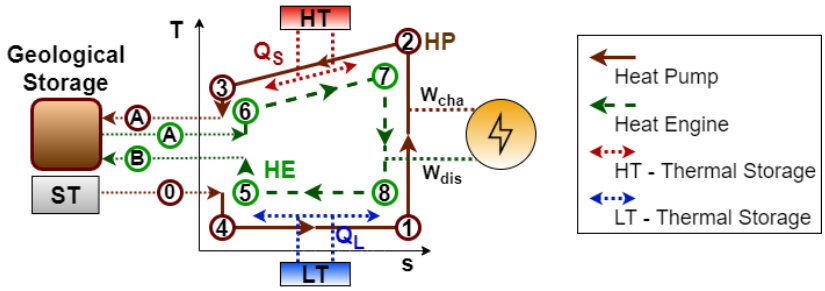

Figure 3. TEES with transcritical cycles adaptation concept including geological CO_2 storage. HT: High-Temperature; LT: Low-Temperature; ST: Stationary Source; Q_S: Sensible Heat; Q_L: Latent Heat; W: Work; cha: Charge; dis: Discharge.

Figure 3 shows the conceptual scheme of the integrated system, the so-called Geological Storage System (GSS) consists of two open and independent CO_2 cycles, connected directly by the geological storage and indirectly by thermal storage. The charge cycle starts with the CO_2 captured in a stationary source, which is transported at high pressure (~100 bar) to the GSS, where it is previously stored in a steel tank. As in the base case system (Figure 1), during periods of excess electricity generation, an electric motor drives the compressor of a heat pump system, transferring electrical energy that is transformed into thermal energy at high and low temperature, in the condenser and evaporator respectively, where is stored. The cooled CO_2 is delivered to an injection well (well A) and injected into a vertically sealed (by a very low permeability cap-rock), porous geological formation at a minimum depth of 800 m, which supposes mechanical energy storage. Within the reservoir, the CO_2 will be heated (small geothermal gain) to balance with the

reservoir temperature, and its density will decrease (thermosiphon). For extraction, well A works as a CO_2 production well. Figure 4 shows the conceptual layout of the system at the charging cycle.

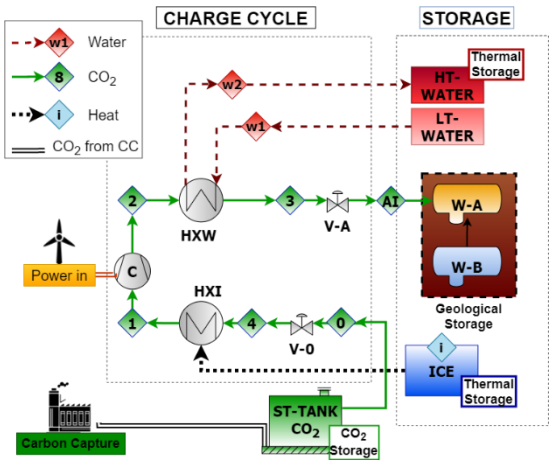

Figure 4. Layout of the charge cycle in the electrothermal energy storage system with geological CO_2 storage (GSS). C: Compressor; V: Valve; HXW: Heat exchange – Water; HXI: Heat exchange – Ice; HT: High Temperature; LT: Low temperature; W: Well; ST: Steel.

During periods of net electricity demand from the grid, electricity is generated from the evolution of the CO_2 stored through a gas turbine, where the expanded fluid is cooled from the previously-stored low-temperature heat source. CO_2 is then injected in the secondary well (well B), located hundreds of meters from the main well (well A), but in the same geological reservoir. Part of the CO2 injected into well B migrates out of wells B and A, and is permanently sequestered in the geological formation, reducing total emissions from stationary CO_2 sources. The remaining CO_2 migrates to well A (due to the thermosiphon), is heated throughout the process and is recovered in the following discharge phases. Figure 5 shows the layout of the GSS during the discharging phase.

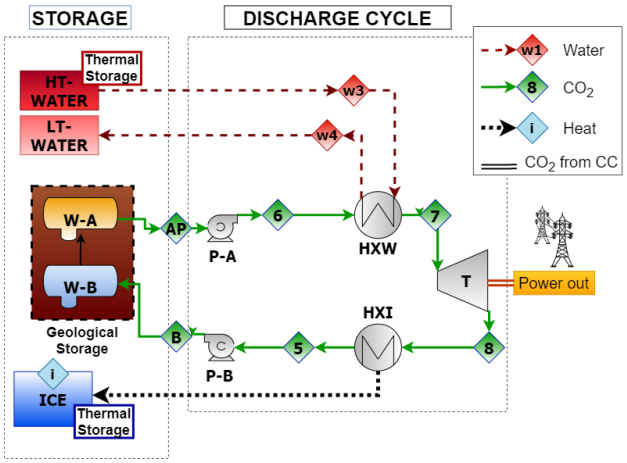

Figure 5. Layout of the discharge cycle in the electrothermal energy storage system with geological CO_2 storage (GSS). P: Pump; T: Turbine; HXW: Heat exchange – Water; HXI: Heat exchange – Ice; HT: High Temperature; LT: Low temperature; W: Well; ST: Steel

3.2 Geological CO_2 storage model

In the geological storage of CO_2, the injection pressure is set as a function of the depth of the geological formation, assumed initially to be at hydrostatic pressure. The CO_2 extraction conditions, which depend on the characteristics of the geological formation, will be at slightly lower pressure and higher temperature than the injection pressure. The values associated with the

performance of the equipment considered, which determine the expansion and compression processes are the same as in the previous case. Taking into account the ground-pipe heat exchange coefficient [48], CO_2 temperature is expected to equilibrate with the ground temperature, taken as 12ºC, during most of the transport process. The pressure during transport and injection is set at 100 bar [49]. In that condition, the fluid is in a phase known as 'dense state', close to a supercritical state.

To ensure a proper operation, independent of the capture CO_2 transport conditions, an expansion valve will be used to adapt the CO_2 to the characteristics demanded by the transcritical CO_2 cycle. In order to obtain results that could be compared with the base case (closed CO_2 transcritical cycles), the high and low charging and discharging pressure values are maintained (Table 2). Since these values may not be optimal for coupling the system with the mechanical storage in the geological formations, an analysis of the variation of the system performance depending on the depth of the well and the pressures of the high and discharge cycles is present in section 5.2. In order to work with different pressure values in wells and heat exchangers, expansion/compression elements are incorporated into the cycle to adapt the pressure values.

Table 2. Main assumptions, inputs and hypothesis on the GSS modelling (see Figure 4 & Figure 5). HP: High-Pressure; LP: Low-Pressure; Ext: Extraction wellhead; Inj: Injection wellhead.

Parameter	Equipment	Unit	Value
Turbomachinery isentropic efficiency	Compressor		0.86
	Pumps		0.85
	Turbine		0.88
Initial conditions in tanks	Water-Pressure	[bar]	100
	Water-Temperature	[ºC]	15
	Ice-Pressure	[bar]	100
	Ice-Temperature	[ºC]	-5
Modelling input parameters	CO_2 quality - compressor		1
	CO_2 quality - pump		0
Heat exchangers	Design pinch point	[ºC]	4
Pressure in cycles	HP of CO_2 in charge	[bar]	200
	LP of CO_2 in charge	[bar]	35
	HP of CO_2 in discharge	[bar]	190
	LP of CO_2 in discharge	[bar]	20
Transport conditions	CO_2-Temperature	[C]	12
	CO_2-Pressure	[bar]	100
Geological storage conditions	Inj-P	[bar]	90/140
*Depth: 1800/3000 meters	Ext-P	[bar]	84.4/135
	Ext-T	[ºC]	37.6/71.1

Injection conditions in the CO_2 main well are imposed by the depth of the reservoir and the need to ensure that no additional compression is required to inject the CO_2. Assuming that the reservoir has adequate permeability and porosity conditions, CO_2 should reach the bottomhole and reservoir at pressure values higher than hydrostatic to ensure injection conditions, as this will improve the overall performance of the system. For reservoir depth limits of 1800 - 3000 meters, wellhead pressure values of 5 to 6 MPa (with the CO_2 column in the well accounting for the increase in pressure necessary to attain the bottomhole pressure) and temperatures of 10 to 20 ºC provide the conditions for the development of a thermosiphon operation.

Table 3. Linear dependence between depth and wellhead pressure considered.

Ext: Extraction wellhead; Inj: Injection wellhead; T: Temperature; P: Pressure; W-A: Main Well.

Depth [m]	Inj-P W-A [bar]	Ext-P W-A [bar]	Ext-T W-A [ºC]
1800	90	83,4	37,6
2100	102,5	96,3	45,98
2400	115	109,2	54,35
2700	127,5	122,1	62,73
3000	140	135	71,1

Assuming that equilibrium is reached between the charging and discharging phases, the extraction conditions of the main well are a function of depth (and indirectly of hydrostatic pressure and geothermal gradient). In order to not limit the study to a specific well depth, a linear dependence between depth and pressure is established as an approximation for a homogeneous reservoir (Table 3), extrapolating to obtain the necessary injection and extraction pressures. Table 3 indicates required wellhead pressures, while bottomhole pressure (higher than reservoir pressure) induced by the CO_2 column is computed assuming that flow in the wells is adiabatic and considering CO_2 density variation and frictional pressure losses as a function of flow rate and well diameter [50]. This approach should be revised if the model is extended to non-homogenous geological sequences or for transient pressure variation.

Analogous to EESS system presented in section 2, different indicators (equations 4-8) are used to determine system performance. Two situations are considered for the charge cycle (COP_{HP}) and overall (η) performance: configurations in which the expansion is not used, and expansion valves are considered, suffix EV; and cases in which the additional expansion could be used in expanders/turbines, EXP

$$COP_{HP,EV} = \frac{\dot{Q}_{HXW} + \dot{Q}_{HXI} + \dot{Q}_{W-A}}{\dot{W}_C} \quad (4)$$

$$COP_{HP,EXP} = \frac{\dot{Q}_{HXW} + \dot{Q}_{HXI} + \dot{Q}_{W-A}}{\dot{W}_C - \dot{W}_{V0-A}} \quad (5)$$

$$\eta_{HE} = \frac{\dot{W}_T + \dot{W}_{PA-B}}{\dot{Q}_{HXW} - \dot{Q}_{HXI}} \quad (6)$$

$$\eta_{EV} = \frac{\dot{W}_T + \dot{W}_{PA-B}}{\dot{W}_C} \quad (7)$$

$$\eta_{EXP} = \frac{\dot{W}_T + \dot{W}_{PA-B}}{\dot{W}_C - \dot{W}_{V0-A}} \quad (8)$$

Where $\dot{Q}_{HXW}, \dot{Q}_{HXI}, \dot{Q}_{W-A}, \dot{W}_{PA-B}$ are the heat power in water and ice heat exchangers and the geothermic gain in wells A and B, respectively, and $\dot{W}_C, \dot{W}_{V0-A}, \dot{W}_T, \dot{W}_{PA-B}$ are the power in compressor, valves, turbine and pumps.

4. ELECTROTHERMAL ENERGY STORAGE SYSTEM BASED ON TRANSCRITICAL CO_2 CLOSED CYCLES AND GEOLOGICAL STORAGE

In the two previous sections, the concepts used for adaptation of the transcritical CO_2 cycles incorporating geological storage have been presented. The previous system, of high interest for being integrated as energy storage from renewables to support CO_2 capture, depends on a continuous CO_2 supply for operation and does not take advantage of the expansion work that occurs in the hydraulic turbine during charge.

Combining in parallel the electrothermal and the geological systems, taking advantage of the common elements, provides an alternative path that closes the cycle for CO_2, and it can be used when there is no availability in the supply of CO_2 from a stationary source, eliminating the

limitation in operation, taking into account only the replacement of the CO_2 fixed in the terrain. This can be easily solved with a discontinuous supply from external sources. The same occurs in the discharge cycle, where the cycle is closed by the pump, and although it causes an imbalance in the discharge of the hot water tank, that means a surplus of stored energy, as occurred in the geological storage system.

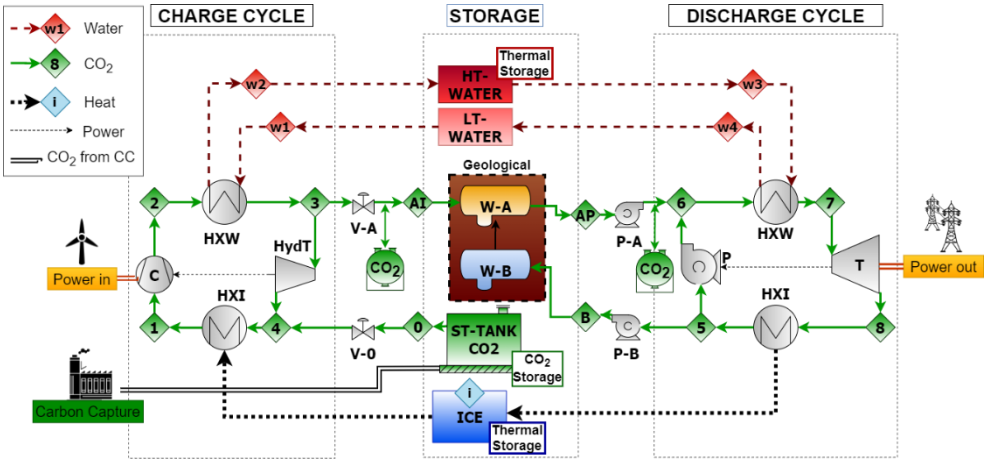

Figure 6. Conceptual layout of charge and discharge cycle in the final integrated system (CEEGSS). C: Compressor; V: Valve; HydT: Hydraulic Turbine; P: Pump; T: Turbine; HXW: Heat exchange – Water; HXI: Heat exchange – Ice; HT: High Temperature; LT: Low temperature; W: Well; ST: Steel.

The proposed integration for the integrated combined system, the CO_2 based electrothermal energy and geological storage system (CEEGSS), is shown in Figure 6. This plant layout integrates geological storage in parallel with expansion during charge and compression during discharging. Four independent operation modes are considered for the operation of the system (Figure 7), two in each cycle: operation as a closed cycle (EESS), and operation as an open cycle (an adaptation of the transcritical cycles by incorporating geological storage - GSS). So, the charge cycle can operate either as an open or close cycle, by injecting or not CO_2 into the well while storing thermal energy in hot water and ice reservoirs, according to whether a supply of captured CO_2 is available, independently of the discharge cycle operation mode, which depends on the level and conditions of the CO_2 stored in the geological formation. This means that they could operate simultaneously; for example, the charge cycle could be operating as an open cycle while the discharge cycle operates as a closed cycle or the opposite.

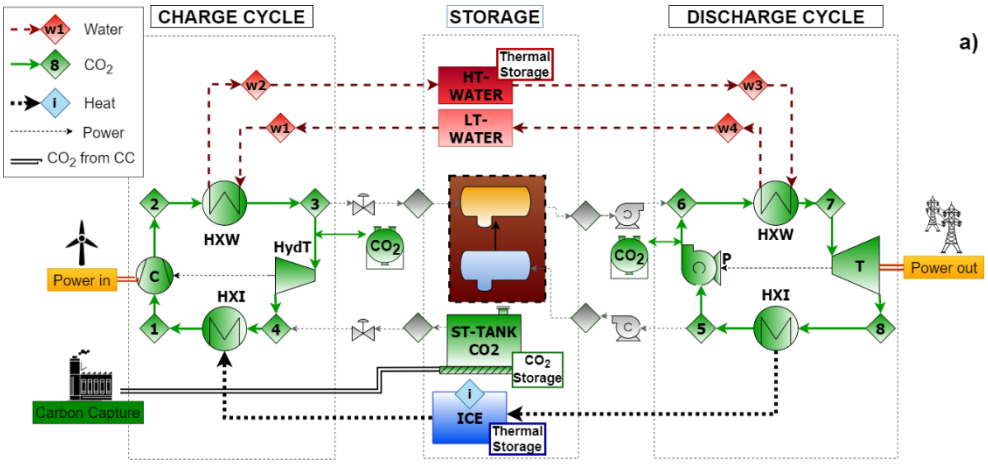

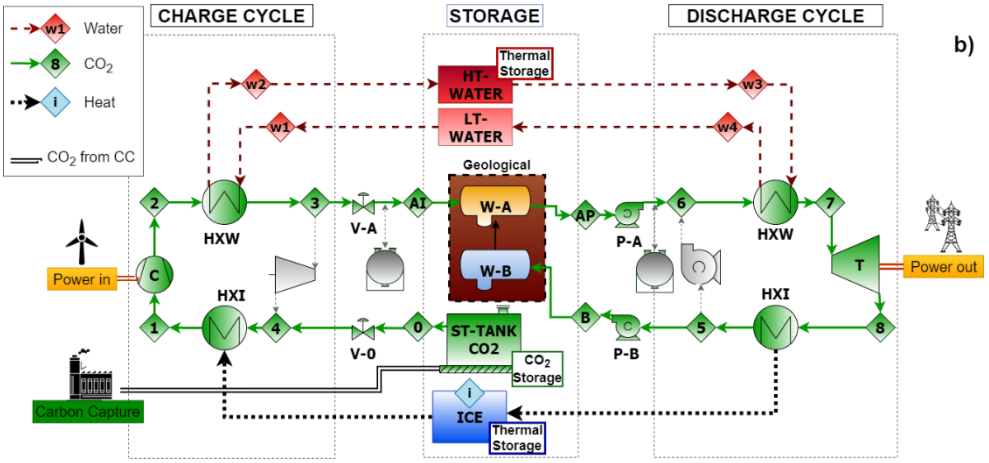

Figure 7. Conceptual layout of the CEEGSS operating as: a) Electrothermal (EESS) charge & discharge cycles b) Geological (GSS); charge & discharge cycles. C: Compressor; V: Valve; Hydraulic Turbine; P: Pump; T: Turbine; HXW: Heat exchange – Water; HXI: Heat exchange – Ice; HT: High Temperature; LT: Low temperature; W: Well; ST: Steel.

5. SYSTEM ANALYSIS AND RESULTS

This section shows the results obtained with the use of the models presented in the previous sections.

5.1 Transcritical CO_2 system for energy storage

For the base case presented in section 2, the energy storage plant is modelled and simulated with the inputs provided in Table 1.

Figure 8 shows the T-s diagram of CO_2 in the base case (EESS). Optimised heat integration is achieved between the cycle and the storage at high temperature, although at low temperature the heat integration can be improved. Note that the potential latent heat is not considered because ice does not change its state. If considered, the latent heat released at low temperature could lead to a significant improvement in system performance, since it would allow reducing the distance between the low-pressure temperature lines in the charge and discharge processes, reducing heat exchange irreversibilities, increasing the enthalpy drop available in the turbine and decreasing it for the compressor. Figure 9 shows the T-Q profiles in the heat exchange process with the heat storage tanks in the charge and discharge processes at high and low temperature

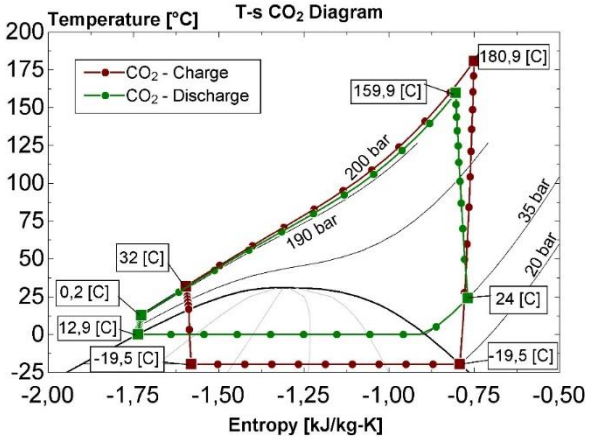

Figure 8. T-s diagram of the EESS by transcritical CO_2 cycles.

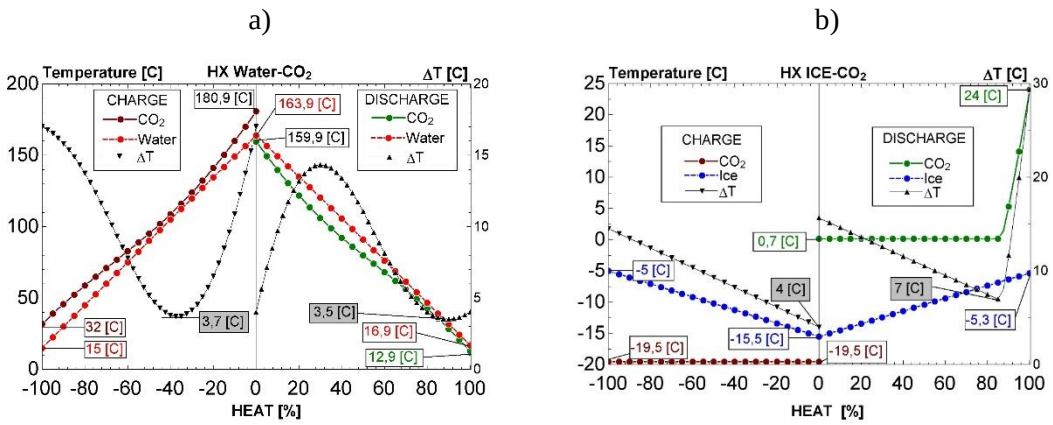

Figure 9. Temperature evolution profile in EESS heat exchanges: a) water-CO_2; b) ice-CO_2

In the heat exchange between the CO_2 and the water tank (Figure 9-a), although there is an adequate integration between the storage and the cycle, the temperature lines of CO_2 and water evolve slightly differently due to the transcritical CO_2 characteristics. In the charge, the pinch point is located near the middle of the heat exchange, which results in a loss of efficiency in the exchange process (resulting in a lower temperature at turbine inlet). At the discharge, the pinch point is located very close to one of the two ends, which enhances the thermal efficiency of the cycle. In the heat exchange between CO_2 and ice, sensible heat is exchanged by the ice, it is cooled at the charge and heated at the discharge, decreases and increases its temperature respectively, while the CO_2 changes its state, with evolution at constant temperature along with the state change.

Table 4. Results – Energy balance on EESS. HXW: Heat Exchange-Water; HXI: Heat Exchange-Ice.

Reference	Work	Charge	Discharge	Power	Charge	Discharge
CO_2 mass flow rate	[kg/s]	1	1	[kg/s]	889,1	1.755
Electrical energy to be stored/released	[kJ/kg]	111.38	57.56	[MW]	100	100
HXW	[kJ/kg]	311.3	323.5	[MW]	276.77	567.83
HXI	[kJ/kg]	199.9	266	[MW]	177.77	466.81
Compression	[kJ/kg]	133.8	19.21	[MW]	118.94	33.72
Expansion	[kJ/kg]	22.42	76.77	[MW]	19.94	134.73
Cycle performance	(Eq. 1-2)	4.595	9.7 %		4.595	9.7
Overall performance	(Eq. 3)	51.6 %			51.6 %	

The heat exchanged is balanced between charge and discharge cycles in the case of hot water. However, in the case of ice, the discharge cycle CO_2 transfers 33% more heat than ice transfers to CO_2 in the charge. This causes an imbalance in the load level of the tanks that must be externally balanced. The analysed Electrical Energy Storage (EESS) results in an overall efficiency of 51.6%.

Sensitivity analysis of the system efficiency

To analyse the effect of different component efficiencies on the performance of the CO_2 storage, a sensitivity analysis for isentropic turbine and compressor efficiencies has been developed. Both have been changed simultaneously to the same value for simplifying representation. The references values were taken from previous transcritical CO_2 cycles studies [31,32]. Figure 10 shows the evolution in charge and discharge efficiency of the cycle as a function of the isentropic efficiencies of turbine and compressor.

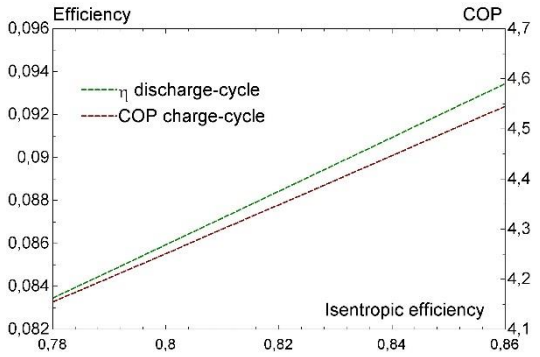

Figure 10. Variation of efficiency in the charge and discharge cycle as a function of compressor and turbine isentropic efficiencies.

In Figure 10 can be seen how the drop in performance of both elements affects the performance of the system because although the performance of the discharge cycle is only reduced by 1%, together with the drop in the COP of the charge cycle (falling below 4.2), it does have a considerable impact on the overall performance of the system.

5.2 Geological CO_2 storage system using transcritical cycles

This section shows the results obtained from the simulation of the GSS model presented in section 3. Depending on the depth of the well, the system evolution varies. In Figure 11 is presented the T-s diagram of the process, where it can be seen how the system with geological storage is formed by two open cycles, in an open-loop process where starting point and ending point of the cycles differ, or the double expansion in the charge and the double compression in the discharge, to adapt the transport/injection/extraction conditions to those of the cycle, as well as the geothermal heat gain within the geological formation.

The charge cycle ends with the injection of the CO_2 into the main well. The greater the depth, the higher the injection pressure required and operating temperature, which leads to higher efficiency. Pre-injection expansion is reduced, but post-extraction compression has much more influence on the overall performance. The higher the outlet temperature of the main well, the compression occurs in a zone located more to the right in the T-s diagram, which makes the inlet temperature higher in the exchange with the hot water, and consequently the final temperature of the hot water will also be higher. This causes an imbalance between the hot water at the start of the process (15ºC) and at the end (>80ºC). It is reflected in additional heat losses as it must be externally dissipated not taking advantage of this heat.

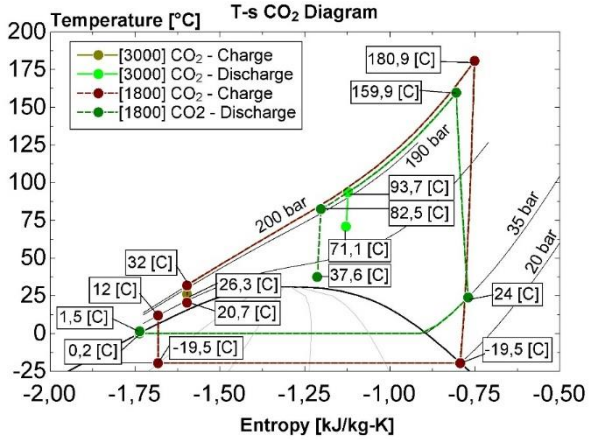

Figure 11. T-s diagram of the CO_2 GSS as a function of depth; 1800 & 3000 m.

a) b)

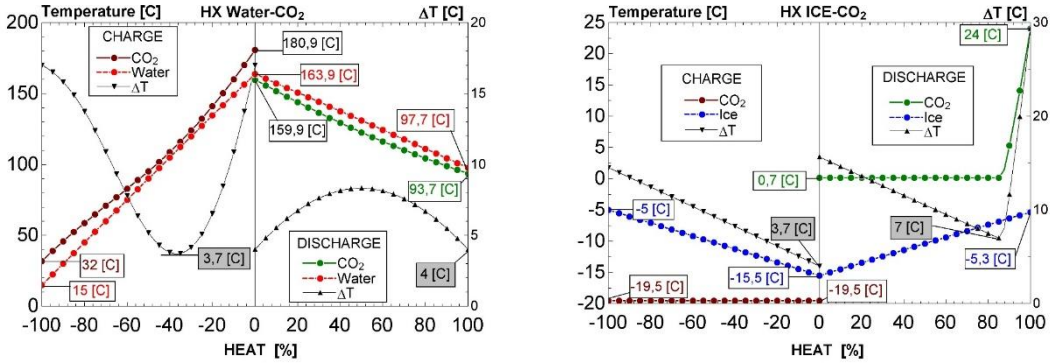

Figure 12. Temperature evolution profile in GSS heat exchanges for 3000 m depth: a) water- CO_2; b) ice- CO_2.

By incorporating storage in geological formations, there is a reduction of the heat exchanged at the discharge of the hot water tank, due to the increase in temperature of the CO_2 leaving the main well. This will cause an imbalance in the temperature of the hot water tank, between charge and discharge, as the heat exchanged in the charging process is approximately twice as much as in the discharge. This is further accentuated by increasing the depth of the well, being 146.9% greater if an injection depth of 3000 m is considered. The inclusion of geological storage hardly affects the main global values of the system. The most significant influence is seen in the work of the first pump, since the expansion lines are distanced by moving to the right in the T-s diagram, Figure 11, and the outlet temperature of well A is higher than the outlet temperature of the condenser. This phenomenon decreases significantly with the increase of well A depth.

*Table 5. Results - Influence of depth in GSS. Ext: Extraction; Inj: Injection; T: Temperature; W-A: Main Well; FR: Flow Rate; HXW: Heat Exchange-Water. LT: Low T. *Mass flow per unit of working fluid*

Depth W-A	**[m]**	**1800**	**2100**	**2400**	**2700**	**3000**
Inj-T W-A	[ºC]	20,7	22,2	23,6	24,9	26,2
Ext-T W-A	[ºC]	37,6	45,9	54,3	62,7	71,1
CO_2-T in HXW	[ºC]	82,5	84,6	89,5	90,6	93,7
LT-Water	[ºC]	86,5	88,6	91,5	94,6	97,7
FR-Water	[kg/kg_{co2}]*	0,473	0,468	0,462	0,455	0,449

The overall efficiency increases from 37% to 45.4% by increasing the depth of well A from 1800 to 3000 meters when not considering the work that could be obtained by taking advantage of the available pressure drop in the expansion valves. If we consider the expansion work, integrating expanders, with additional cost, the yield increases from 45% at 1800 meters depth to 52.7% at 3000 m.

Table 6. Results – Energy balance and performance on GSS model. FR: Flow Rate; PW: Power; HXW: Heat Exchange-Water; HXI: Heat Exchange-Ice; ΔQ W-A/B: Theoretical in-well geothermal gain; COMP: Compressor; TURB: Turbine; V: Valve; P: Pump; PERF: Performance; EXP/EV: Performance of the system evaluating/no evaluating work in the double expansion

	Reference	Charge					Discharge				
Depth W-A	[m]	1800	2100	2400	2700	3000	1800	2100	2400	2700	3000
FR – CO_2	[kg/s]	1					1				
HXW	[kJ/kg]	311.3					155	149.5	141.7	133.8	126.1
HXI	[kJ/kg]	225.7					266				
ΔQ W-A/B	[kJ/kg]	116	122.9	131.9	141.2	150.5	160.2	168.7	179.1	189.9	200.6
COMP/TURB	[kJ/kg]	133.8					76.77				
V-0/P-A	[kJ/kg]	11.65					25.67	22.71	19.98	17.15	14.18
V-A/P-B	[kJ/kg]	12.78	11.3	9.82	8.35	6.89	1.9				
Cycle-PERF EV	(Eq. 4)	4.01					0.117	0.125	0.134	0.144	0.155
Cycle-PERF EXP	(Eq. 5-6)	4.91	4.84	4.78	4.72	4.66					
Overall-PERF EV	(Eq. 7)	0.37	0.39	0.41	0.431	0.454					
Overall-PERF EXP	(Eq. 8)	0.45	0.47	0.489	0.507	0.527					

By comparing the performance of the EESS and GSS under optimised pressure for EESS conditions, the performance in the case of geological storage at 3000 meters, considering the use of the available pressure drop with expanders/turbines, it increases from 51.6% in EESS to 52.7% in GSS.

Influence of pressure values

In order to analyse the effect of the different operating conditions on the performance of CO_2 storage, a parametric analysis for high-pressure CO_2 is performed, with particular emphasis on pressure values lower than considered in the geological formation. At an injection depth of 1800 m, with a temperature considered in the reservoir of 37.6 ºC, the pressure values lower than the injection/extraction values require a pre-injection compression, which also causes in most cases that the CO_2 is injected at a higher temperature than is considered in the geological formation, due to the nature of the fluid, whose critical temperature (31 ºC) is very close to the one considered in the reservoir (37.6 ºC), so cooling in the reservoir would be experimented. Only the range of values between the critical pressure of CO_2 (74.5 bar) and the considered extraction pressure (83.4 bar) would be safe from this adverse effect. As the depth of the well increases, the temperature of the reservoir and the considered extraction pressure increase, and with them, the interval between the critical pressure and the extraction pressure. For a well depth of 3000 m, the reservoir temperature would be 71.1 ºC, with an extraction pressure of 135 bar, so that for all values of high CO_2 pressure between extraction and critical pressure, an additional compression would be required prior to injection, and cooling inside the reservoir would not happen.

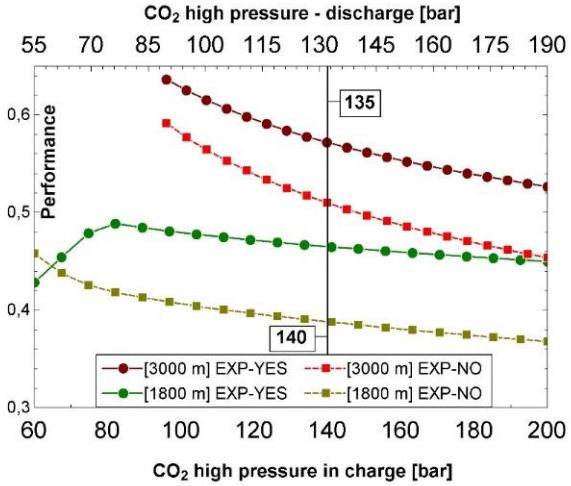

Figure 13. Variation of system performance as a function of pressure values in GSS. EXP YES/NO: Performance of the system evaluating/not evaluating work in double expansion.

As for the influence on the overall performance of the system, an improvement is observed by decreasing the high CO_2 pressures in the charge and the discharge. According to the overall performance indicator, defined in equation 6, the performance increases as the pressures decrease; this makes it clear that the optimised pressures of the EESS (Table 1) were not optimal for evaluating the performance in the system with geological storage.

5.3 An integrated energy storage system with transcritical CO_2 closed cycles and geological storage

The third system presented in section 4 is a combination of the two previous ones. In the T-s diagram of Figure 14, the closed cycles (EESS) begin and end at the same point, while the open cycles (GSS) depend on the depth of the geological formation.

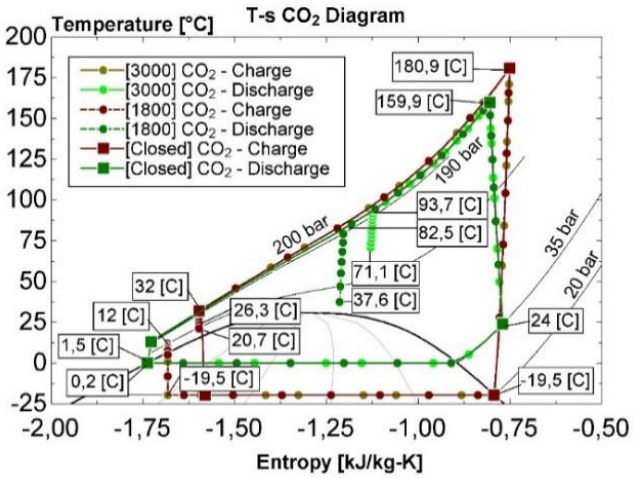

Figure 14. T-s diagram of the CEEGSS. [3000] & [1800]: Depth (m) in CEEGSS system operating as GSS; [Closed] CEEGSS system operating as ESS.

a) b)

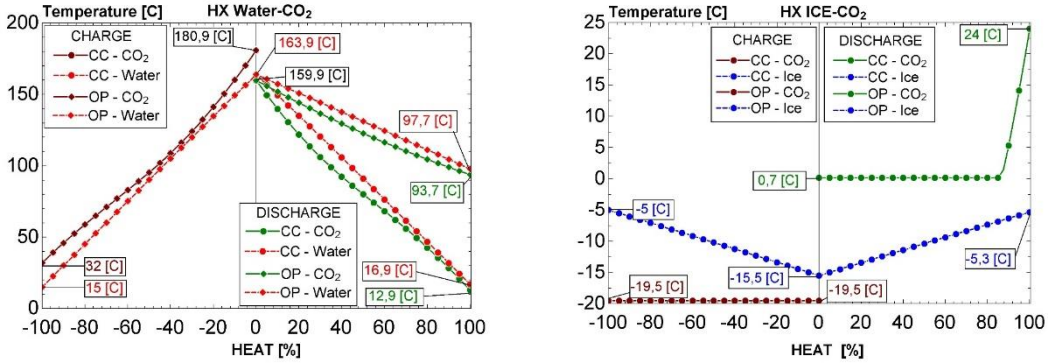

Figure 15. Temperature evolution in CEEGSS heat exchanges: a) water- CO_2 (high temperature); b) ice- CO_2 (low temperature). CC: Close cycle – CEEGSS operating as ESS. OP: Open cycle – CEEGSS operating as GSS

In the heat exchange processes, represented in Figure 15, after the exchange corresponding to the open discharge cycle, an imbalance is produced in the hot water tank and results in a surplus of energy that can be used in other applications or lost to the ambient with a penalty in the efficiency. Table 7 shows the main results of the final system model, referenced to a CO_2 unit mass flow in each cycle, for an injection depth of 3000 m.

*Table 7. Results – Energy balance and performance for 3000 m depth of well. CEEGSS model. FR: Flow Rate; HXW: Heat Exchange-Water; HXI: Heat Exchange-Ice; PERF: Performance; *Mass flow per unit of working fluid; **Function of the well depth.*

		Operating as ESS		**Operating as GSS**	
		Charge	**Discharge**	**Charge**	**Discharge**
FR – CO_2	[kg/s]	1	1	1	1
FR – Water	[kg/kg_{co2}]*	0.5	0.52	0.5	0.45**
FR – Ice	[kg/kg_{co2}]*	9.37	9.7	9.37	10.6
Power	[kW]	114.8	55.65	118.8**	58.72**
HXW	[kJ/kg]	311.3	323.5	311.3	126.1**
HXI	[kJ/kg]	199.9	266	225.7	266
Compression	[kJ/kg]	133.8	19.21	133.8	16.08**
Expansion	[kJ/kg]	22.42	76.77	18.54**	76.77
PERF-Cycle		4,59	0,097	5,97**	0,155**
PERF-Overall		0,517		0,527**	

The results confirm that the CEEGSS integrates both the characteristics of the EESS and those of the GSS, offering one or the other depending on the mode of operation.

6. TIME ANALYSIS EVOLUTION

In order to show system operation and integrated system behaviour, different profiles were simulated based on data profiles of wind, solar generation and CO_2 capture in a stationary source. They were used to build operation profiles in the charge cycle (energy storage) and discharge cycle (electricity generation), based on existing data, showing the alternating operation between open cycle (EESS and GSS) and closed-cycle (EESS only).

6.1 Scenario I: Hourly Electricity Price

In this first scenario, a plant with an electrical output power of 1.500 kW is considered and an electrical input power of 2.000 kW. This difference is intended to provide a nominal mass flow of charge and discharge of similar value, about 15-20 kg/s, and several times higher than the captured CO2. From a nearby power plant of 20MWe, a mass flow close to 5 kg/s was considered scaling up data of captured CO2 mass flow in a 150 MWe plant [51].

The main criterion followed in the operation of the system is the price of electricity, according to tariffs with hourly discrimination (Hourly Price of Electricity); during the hours of low price, the charge cycle comes into operation, in which electricity is consumed, either from the grid or of renewable origin, during the hours of high tariff, the discharge cycle comes into operation, in which energy is injected into the grid. Operating mode along a day simulated is represented in Figure 16-a.

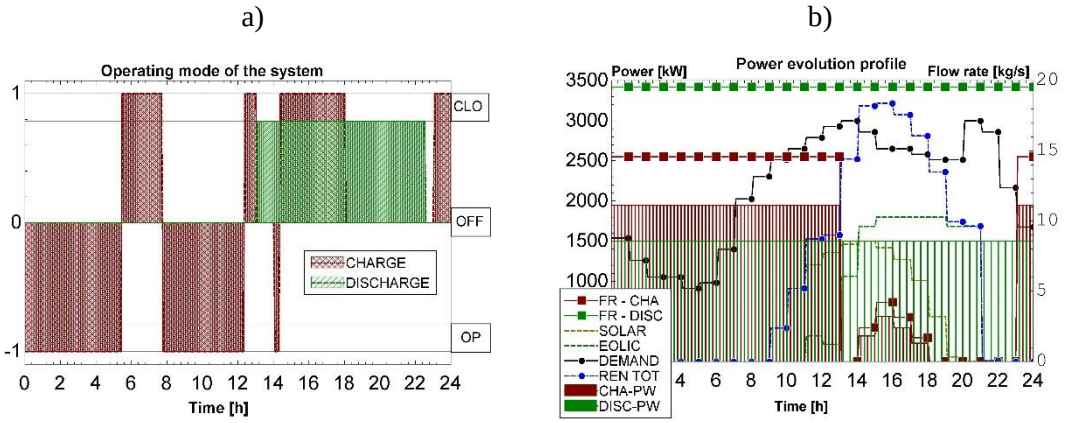

Figure 16. CEEGSS, according to HPE: a) Operating time; b) Power evolution profile. CLO: Closed cycle – CEEGSS operating as ESS. OP: Open cycle – CEEGSS operating as GSS. CHA: Charge; DISC: Discharge; FR: Flow Rate; REN-TOT: Total Renewable power; PW: Power.

When the charging cycle starts, as long as a maximum level is not reached in one of the thermal tanks, the open cycle configuration will be used whenever the CO_2 reaches a certain level in a steel tank. Otherwise, the closed cycle configuration will be used.

A certain level of charge in the ice and hot water tanks is required for the discharge cycle to start, in addition to CO_2 in the well under discharge conditions in the case of the open cycle.

Figure 16-b shows the hourly power: the operation of the system depends primarily on the hourly price of electricity, so the system will operate as a charge cycle (consumer) during off-peak hours, and as a discharge cycle (generator) during high-price hours. Approximately half of the time in each mode of operation covers the requirements in the tanks. During those hours, the system operates in nominal mode, with constant CO_2 mass expenditure, and very similar in charge and discharge. To include the influence of the electricity system in the simulation, an additional condition is added in the operation of the charge cycle; when wind and photovoltaic generation power exceeds a considered demand, the charge cycle is put into operation, at partial load, with the power remaining from the difference between the renewable and the demand.

6.2 Scenario II: Availability Renewable Resource and variable Demand

In this scenario, the charge cycle will start operating according to the availability of wind and solar resources (Availability of Renewable Resource), consuming energy of exclusively renewable origin. Also, the influence of the electricity demand (Availability of Renewable Resource and Demand) curve will affect the discharge cycle, which will condition its operation. A variable has also been included that allows the simulation of the lateral migration of CO_2 inside geological formations, through a loss of a fraction of the total mass of CO_2 inside the well over time.

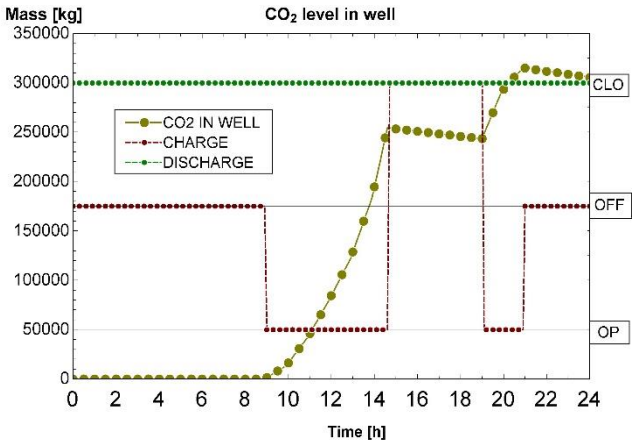

Figure 17. Evolution profile of the CO_2 mass stored into geological formations according to ARRD. CLO: Closed cycle – CEEGSS operating as EESS. OP: Open cycle – CEEGSS operating as GSS.

For the simulation of the plant, a wind farm on a smooth, open-field surface with a nominal power of 1.8 MW is considered, using nine (200 kW) wind turbines, which operate in a westerly direction, start-up at a speed of 3 m/s and reach nominal power at a speed of 12 m/s. The photovoltaic plant considered in the study will have a nominal power of 1.500 kW, using 5.000 photovoltaic modules of 300 W, which corresponds to the hour of maximum production. CO_2 supply is considered the same than in scenario I, and corresponding to the peak in the actual emissions curve [51]. Power evolution along the day simulated is represented in Figure 18-b.

a) b)

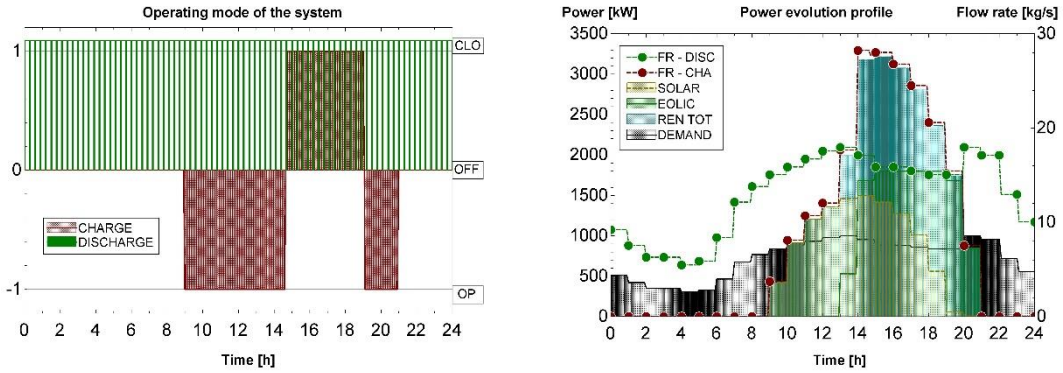

Figure 18. CEEGSS according to ARRD: a) Operating time b) Power evolution profile. CLO: Closed cycle – CEEGSS operating as EESS. OP: Open cycle – CEEGSS operating as GSS. CHA: Charge; DISC: Discharge; FR: Flow Rate; REN-TOT: Total Renewable power.

With the new control criterion, the discharge cycle is in operation throughout the day, following the variable demand for electrical energy. The charge cycle starts when there is the availability of the renewable resource, wind and/or solar, as shown in Figure 18-a.

The system can store energy exclusively from renewable sources, and is capable of following a variable and continuous electrical energy demand, in terms of generation; it also takes advantage of the renewable energy storage process, to store inside a geological formation, the continuous and variable supply of CO_2 captured in a nearby power plant or local industries producers of CO_2.

CONCLUSIONS

Large-scale electrothermal energy storage, based on trans-critical CO_2 cycles and heat transfer to ice and hot water reservoirs, has the potential to be combined with storage of CO_2 in geological formations. The concept is developed in this work through the analysis of three high-performance systems: renewable energy storage using a thermoelectric energy storage system, based on a reversible heat pump; a CO_2 storage system that integrates the thermoelectric storage system; and a novel integration of energy storage using a reversible heat pump and geological injection of CO_2. The system uses sensible heat storage in water and ice storage systems that couple the charge and .discharge cycles.

The presented analyses shows the system is presented as a viable alternative for the storage of electrical energy; with a round trip efficiency close to 50%.

The geological storage system is conceived to operate with CO_2 captured from stationary sources as working fluid for the storage of energy from renewable sources. The energy is stored and recovered while promoting the capture of CO_2, which adds value to the system. The system reaches a yield close to 50%. It would allow using this renewable energy stored in the CO_2 capture process, for instance, making greener the CO_2 capture process.

Geological of CO_2 and energy storage could be integrated with CO_2 capture systems providing an interesting integration of renewables. This system is based on a continuous supply of CO_2 to operate the charge cycle and a stored CO_2 amount (under certain conditions) in the discharge cycle. The parallel integration combining both systems, taking advantage of the shared components and synergies provide benefits in a closed CO_2 loop system, with a fraction of the CO_2 being geologically sequestered.

Regarding the CO_2 injected into the geological formation, it was assumed that a fraction migrates laterally or is trapped and does not return to well A after being injected into well B after the open cycle has been discharged. The rest, the amount stored in the reservoir around well A, follows an increasing trend.

Two scenarios based on renewables generation profiles data were developed in order to show potential operation modes of the proposed system. The analysis of the time evolution of the system, under different operation criteria, shows a favourable response under both scenarios: considering energy storage exclusively from renewable origin and generation according to continuous and fluctuating demand, and the approach of energy storage/generation according to the electricity tariff with hourly discrimination.

The three systems presented have been shown of interest, with high performance, under different integrations: renewable energy storage using a thermoelectric energy storage system, based on a reversible heat pump; integrated into a CO_2 capture system and energy storage, allowing the combination of the CCS and renewables; and a novel integration in CO_2 closed-loop energy storage and geological injection of the CO_2. Future works will be oriented to advance in the study and optimisation of the system, with modifications on the operation of components, integration modes and system applications.

Acknowledgements

This work was partially funded by the project ‘Sistema de almacenamiento termóquímico de energía para plantas solares de concentración- SunStorCa(OH)’, reference P18-RT-1044, by the Regional Government of Andalucia, Junta de Andalucia, and FEDER Regional European Funds.

JC gratefully acknowledges the Portuguese Foundation for Science and Technology (FCT) through project UIDB/04683/2020 - ICT (Institute of Earth Sciences).

REFERENCES

[1] Renewable Energy Agency I. 2050 ENERGY TRANSFORMATION EDITION: 2020 GLOBAL RENEWABLES OUTLOOK. 2020.

[2] Urzúa IA, Olmedo JC, Sauma EE. Impact of intermittent non-conventional renewable generation in the costs of the Chilean main power system. Renewable and Sustainable Energy Reviews 2016;60:810–21. doi:10.1016/j.rser.2016.01.124.

[3] Nobela ON, Bansal RC, Justo JJ. A review of power quality compatibility of wind energy conversion systems with the South African utility grid. Renewable Energy Focus 2019;31:63–72. doi:10.1016/j.ref.2019.10.001.

[4] Chen H, Cong TN, Yang W, Tan C, Li Y, Ding Y. Progress in electrical energy storage system: A critical review. Progress in Natural Science 2009;19:291–312. doi:10.1016/j.pnsc.2008.07.014.

[5] de Carvalho WC, Bataglioli RP, Fernandes RAS, Coury D V. Fuzzy-based approach for power smoothing of a full-converter wind turbine generator using a supercapacitor energy storage. Electric Power Systems Research 2020;184:106287. doi:10.1016/j.epsr.2020.106287.

[6] Hutchinson A, Gladwin DT. Optimisation of a wind power site through utilisation of flywheel energy storage technology. Energy Reports, vol. 6, Elsevier Ltd; 2020, p. 259–65. doi:10.1016/j.egyr.2020.03.032.

[7] Boparai KS, Singh R. Electrochemical Energy Storage Using Batteries, Superconductors and Hybrid Technologies. Encyclopedia of Renewable and Sustainable Materials, Elsevier; 2020, p. 248–54. doi:10.1016/b978-0-12-803581-8.11277-9.

[8] Figgener J, Stenzel P, Kairies KP, Linßen J, Haberschusz D, Wessels O, et al. The development of stationary battery storage systems in Germany – A market review. Journal of Energy Storage 2020;29. doi:10.1016/j.est.2019.101153.

[9] Lovegrove K, James G, Leitch D, Milczarek A, Ngo A, Rutovitz J, et al. Comparison of Dispatchable Renewable Electricity Options: Technologies for an orderly transition 2018.

[10] Yang TF, Lu JH, Yan WM, Ghalambaz M. Optimization of pulse current on energy storage of zinc-air flow batteries. Journal of Power Sources 2019;442:227253. doi:10.1016/j.jpowsour.2019.227253.

[11] Marzebali MH, Mazidi M, Mohiti M. An adaptive droop-based control strategy for fuel cell-battery hybrid energy storage system to support primary frequency in stand-alone microgrids. Journal of Energy Storage 2020;27:101127. doi:10.1016/j.est.2019.101127.

[12] Cheng C, Blakers A, Stocks M, Lu B. Pumped hydro energy storage and 100 % renewable electricity for East Asia. Global Energy Interconnection 2019;2:386–92. doi:10.1016/j.gloei.2019.11.013.

[13] Ramadan O, Omer S, Ding Y, Jarimi H, Chen X, Riffat S. Economic evaluation of installation of standalone wind farm and wind + CAES system for the new regulating tariffs for renewables in Egypt. Thermal Science and Engineering Progress 2018;7:311–25. doi:10.1016/j.tsep.2018.06.005.

[14] Ochs F, Dahash A, Tosatto A, Bianchi Janetti M. Techno-economic planning and construction of cost-effective large-scale hot water thermal energy storage for Renewable District heating systems. Renewable Energy 2020;150:1165–77. doi:10.1016/j.renene.2019.11.017.

[15] Denholm P, Holloway T. Improved accounting of emissions from utility energy storage system operation. Environmental Science and Technology 2005;39:9016–22.

doi:10.1021/es0505898.

[16] Llamas B, Ortega MF, Barthelemy G, de Godos I, Acién FG. Development of an efficient and sustainable energy storage system by hybridisation of compressed air and biogas technologies (BIO-CAES). Energy Conversion and Management 2020;210:112695. doi:10.1016/j.enconman.2020.112695.

[17] Bullough C, Gatzen C, Jakiel C, Koller M, Nowi A, Zunft S. Advanced Adiabatic Compressed Air Energy Storage for the Integration of Wind Energy. 2004.

[18] Jacob R, Belusko M, Liu M, Saman W, Bruno F. Using renewables coupled with thermal energy storage to reduce natural gas consumption in higher temperature commercial/industrial applications. Renewable Energy 2019;131:1035–46. doi:10.1016/j.renene.2018.07.085.

[19] Schmidt T, Pauschinger T, Sørensen PA, Snijders A, Djebbar R, Boulter R, et al. Design Aspects for Large-scale Pit and Aquifer Thermal Energy Storage for District Heating and Cooling. Energy Procedia, vol. 149, Elsevier Ltd; 2018, p. 585–94. doi:10.1016/j.egypro.2018.08.223.

[20] Cetin TH, Kanoglu M, Yanikomer N. Cryogenic energy storage powered by geothermal energy. Geothermics 2019;77:34–40. doi:10.1016/j.geothermics.2018.08.005.

[21] Javed F, Ullah F, Zakaria MR, Akil HM. An approach to classification and hi-tech applications of room-temperature ionic liquids (RTILs): A review. Journal of Molecular Liquids 2018;271:403–20. doi:10.1016/j.molliq.2018.09.005.

[22] Alptekin E, Ezan MA. Performance investigations on a sensible heat thermal energy storage tank with a solar collector under variable climatic conditions. Applied Thermal Engineering 2020;164:114423. doi:10.1016/j.applthermaleng.2019.114423.

[23] Laing D, Zunft S. Using concrete and other solid storage media in thermal energy storage (TES) systems. Advances in Thermal Energy Storage Systems: Methods and Applications, Elsevier Inc.; 2015, p. 65–86. doi:10.1533/9781782420965.1.65.

[24] Prieto C, Cabeza LF. Thermal energy storage (TES) with phase change materials (PCM) in solar power plants (CSP). Concept and plant performance. Applied Energy 2019;254:113646. doi:10.1016/j.apenergy.2019.113646.

[25] Javed MS, Ma T, Jurasz J, Amin MY. Solar and wind power generation systems with pumped hydro storage: Review and future perspectives. Renewable Energy 2020;148:176–92. doi:10.1016/j.renene.2019.11.157.

[26] Rahmanifard H, Plaksina T. Hybrid compressed air energy storage, wind and geothermal energy systems in Alberta: Feasibility simulation and economic assessment. Renewable Energy 2019;143:453–70. doi:10.1016/j.renene.2019.05.001.

[27] Steinmann W-D, Jockenhöfer H, Bauer D. Thermodynamic Analysis of High-Temperature Carnot Battery Concepts. Energy Technology 2020;8:1900895. doi:10.1002/ente.201900895.

[28] Marguerre F. Ueber ein neues Verfahren zur Aufspeicherung elektrischer Energie. Mitteilungen Der Vereinigung Der Elektrizitätswerke 1924;354:27E35.

[29] Cahn RP. United States Patent (19) Cahn THERMAL ENERGY STORAGE BY MEANS OF REVERSIBLE HEAT PUM.PNG. 1976.

[30] Patent US. Thermal energy storage by means of reversible heat pumping utilising industrial waste heat. 1977.

[31] Mercangöz M, Hemrle J, Kaufmann L, Z'Graggen A, Ohler C. Electrothermal energy storage with transcritical CO2 cycles. Energy 2012;45:407–15. doi:10.1016/j.energy.2012.03.013.

[32] Fernandez R, Chacartegui R, Becerra A, Calderon B, Carvalho M. Transcritical carbon dioxide charge-discharge energy storage with integration of solar energy. Journal of Sustainable Development of Energy, Water and Environment Systems 2019;7:444–65. doi:10.13044/j.sdewes.d6.0235.

[33] Hao Y, He Q, Du D. A trans-critical carbon dioxide energy storage system with heat pump to recover stored heat of compression. Renewable Energy 2020;152:1099–108. doi:10.1016/j.renene.2020.01.099.

[34] Hao Y, He Q, Liu W, Pan L, Oldenburg CM. Thermodynamic analysis of a novel fossil-fuel–free energy storage system with a trans-critical carbon dioxide cycle and heat pump. International Journal of Energy Research 2020;44:7924–37. doi:10.1002/er.5130.

[35] Tesio U, Guelpa E, Verda V. Integration of thermochemical energy storage in concentrated solar power. Part 2: Comprehensive optimisation of supercritical CO2 power block. Energy Conversion and Management: X 2020;6:100038. doi:10.1016/j.ecmx.2020.100038.

[36] Fernández R, Ortiz C, Chacartegui R, Valverde JM, Becerra JA. Dispatchability of solar photovoltaics from thermochemical energy storage. Energy Conversion and Management 2019;191:237–46. doi:10.1016/j.enconman.2019.03.074.

[37] Liu Z, Yang X, Jia W, Li H, Yang X. Justification of CO2 as the working fluid for a compressed gas energy storage system: A thermodynamic and economic study. Journal of Energy Storage 2020;27:101132. doi:10.1016/j.est.2019.101132.

[38] Buscheck TA, Bielicki JM, Randolph JB. CO2 Earth Storage: Enhanced Geothermal Energy and Water Recovery and Energy Storage. Energy Procedia, vol. 114, Elsevier Ltd; 2017, p. 6870–9. doi:10.1016/j.egypro.2017.03.1615.

[39] Li Y, Yu H, Liu Y, Zhang G, Tang D, Jiang Z. Numerical study on the hydrodynamic and thermodynamic properties of compressed carbon dioxide energy storage in aquifers. Renewable Energy 2020;151:1318–38. doi:10.1016/j.renene.2019.11.135.

[40] Child M, Bogdanov D, Breyer C. The role of storage technologies for the transition to a 100% renewable energy system in Europe. Energy Procedia, vol. 155, Elsevier Ltd; 2018, p. 44–60. doi:10.1016/j.egypro.2018.11.067.

[41] Child M, Kemfert C, Bogdanov D, Breyer C. Flexible electricity generation, grid exchange and storage for the transition to a 100% renewable energy system in Europe. Renewable Energy 2019;139:80–101. doi:10.1016/j.renene.2019.02.077.

[42] Rayhan FA, Yanuar, Pamitran AS. Effect of ice mass fraction on ice slurry flow for cold energy storage application. Energy Reports, vol. 6, Elsevier Ltd; 2020, p. 790–4. doi:10.1016/j.egyr.2019.11.159.

[43] Averfalk H, Ingvarsson P, Persson U, Werner S. ON THE USE OF SURPLUS ELECTRICITY IN DISTRICT HEATING SYSTEMS. 2014.

[44] Borri E, Sze JY, Tafone A, Romagnoli A, Li Y, Comodi G. Experimental and numerical characterisation of sub-zero phase change materials for cold thermal energy storage. Applied Energy 2020;275:115131. doi:10.1016/j.apenergy.2020.115131.

[45] Yan J, Zhang X. Application and development of dynamic ice slurry technology. 2010 International Conference on Mechanic Automation and Control Engineering, MACE2010, 2010, p. 1441–4. doi:10.1109/MACE.2010.5536141.

[46] EES: Engineering Equation Solver | F-Chart Software : Engineering Software n.d. http://fchartsoftware.com/ees/ (accessed November 23, 2020).

[47] Morandin M, Maréchal F, Mercangöz M, Buchter F. Conceptual design of a thermo-electrical energy storage system based on heat integration of thermodynamic cycles - Part A: Methodology and base case. Energy 2012;45:375–85.

doi:10.1016/j.energy.2012.03.031.

[48] Svensson R, Odenberger M, Johnsson F, Strömberg L. Transportation systems for CO2 - Application to carbon capture and storage. Energy Conversion and Management 2004;45:2343–53. doi:10.1016/j.enconman.2003.11.022.

[49] Romeo LM, Bolea I, Lara Y, Escosa JM. Optimisation of intercooling compression in CO2 capture systems. Applied Thermal Engineering 2009;29:1744–51. doi:10.1016/j.applthermaleng.2008.08.010.

[50] Adams BM, Kuehn TH, Bielicki JM, Randolph JB, Saar MO. On the importance of the thermosiphon effect in CPG (CO2 plume geothermal) power systems. Energy 2014;69:409–18. doi:10.1016/j.energy.2014.03.032.

[51] Bonaventura D, Chacartegui R, Valverde JM, Becerra JA, Ortiz C, Lizana J. Dry carbonate process for CO2 capture and storage: Integration with solar thermal power. Renewable and Sustainable Energy Reviews 2018;82:1796–812. doi:10.1016/j.rser.2017.06.061.